Glycerol Dehydrogenase: Structure, Specificity, and Mechanism of a Family III Polyol Dehydrogenase

Sergey N. Ruzheinikov, 1 Jacky Burke, 1 Sveta Sedelnikova,1 Patrick J. Baker,1 Robert Taylor,1 Per A. Bullough,1 Nicola M. Muir,² Michael G. Gore,² and David W. Rice^{1,3} ¹Krebs Institute for Biomolecular Research Department of Molecular Biology and Biotechnology University of Sheffield Firth Court Western Bank Sheffield S10 2TN United Kingdom ²Department of Biochemistry and Molecular Biology University of Southampton **Bassett Crescent East** Southampton SO16 7PX **United Kingdom**

Summary

Background: Bacillus stearothermophilus glycerol dehydrogenase (GlyDH) (glycerol:NAD+ 2-oxidoreductase, EC 1.1.1.6) catalyzes the oxidation of glycerol to dihydroxyacetone (1,3-dihydroxypropanone) with concomitant reduction of NAD+ to NADH. Analysis of the sequence of this enzyme indicates that it is a member of the so-called iron-containing alcohol dehydrogenase family. Despite this sequence similarity, GlyDH shows a strict dependence on zinc for activity. On the basis of this, we propose to rename this group the family III metal-dependent polyol dehydrogenases. To date, no structural data have been reported for any enzyme in this group.

Results: The crystal structure of *B. stearothermophilus* glycerol dehydrogenase has been determined at 1.7 Å resolution to provide structural insights into the mechanistic features of this family. The enzyme has 370 amino acid residues, has a molecular mass of 39.5 kDa, and is a homooctamer in solution.

Conclusions: Analysis of the crystal structures of the free enzyme and of the binary complexes with NAD⁺ and glycerol show that the active site of GlyDH lies in the cleft between the enzyme's two domains, with the catalytic zinc ion playing a role in stabilizing an alkoxide intermediate. In addition, the specificity of this enzyme for a range of diols can be understood, as both hydroxyls of the glycerol form ligands to the enzyme-bound Zn²⁺ ion at the active site. The structure further reveals a previously unsuspected similarity to dehydroquinate synthase, an enzyme whose more complex chemistry shares a common chemical step with that catalyzed by glycerol dehydrogenase, providing a striking example of divergent evolution. Finally, the structure suggests

that the NAD⁺ binding domain of GlyDH may be related to that of the classical Rossmann fold by switching the sequence order of the two mononucleotide binding folds that make up this domain.

Introduction

Enzymes termed glycerol dehydrogenases (GlyDH) have been isolated from a number of different organisms including bacteria [1, 2], Neurospora [3], yeast [4, 5], and mammals [6]. These enzymes are divided into three classes depending upon the site of oxidation of the glycerol and the nature of the coenzyme required. In anaerobic conditions, many microorganisms utilize glycerol as a source of carbon through coupled oxidative and reductive pathways [7, 4]. The utilization of glycerol in such a manner is catalyzed by glycerol dehydrogenase (GlyDH) (glycerol:NAD+ 2-oxidoreductase, EC 1.1.1.6) and leads to the formation of dihydroxyacetone (1,3dihydroxypropanone) with concomitant reduction of NAD+ to NADH (Figure 1) [4]. The dihydroxyacetone is then phosphorylated by dihydroxyacetone kinase and enters the glycolytic pathway for further degradation [8].

The GlyDH from the thermophilic bacterium *B. stearothermophilus* is a metallo-enzyme that displays maximum activity between pH 6.0 and pH 8.5 [2]. It consists of one Zn²⁺-dependent polypeptide chain of 370 amino acid residues with a molecular weight of 39.5 kDa [9] and is thought to be a homooctamer in solution [10]. Like the equivalent enzyme from other species, *B. stearothermophilus* GlyDH can utilize various diols such as propan-1,2-diol, butan-2,3-diol, ethan-1,2-diol, and 3-mercapto-1,2-dihydroxypropane [2, 3]. The class of GlyDH to which the *B. stearothermophilus* enzyme belongs shows considerable sequence conservation across species, with, for example, 49% identity between the latter and *Escherichia coli* GlyDHs [11] in a 367-residue overlap (Figure 2).

The NAD+-linked GlyDHs are members of a diverse group of polyol dehydrogenases that can be grouped into three distinct protein families. The first of these families, containing horse-liver alcohol dehydrogenase and human $\beta_1\beta_1$ alcohol dehydrogenase, is the Zn²⁺dependent, "medium-chain" alcohol dehydrogenases, which all have a subunit size that contains approximately 400 residues [12, 13]. The second family of polyol dehydrogenases includes an alcohol dehydrogenase from Drosophila [15], ribitol dehydrogenases [16], mammalian 11 β - and 17 β -hydroxysteroid dehydrogenases [17, 18], and β -ketoreductase [19] and consists of the "shortchain" enzymes [14], based on a subunit of approximately 250 residues. The three-dimensional structure of 3α,20β-hydroxysteroid dehydrogenase from Streptomyces hydrogenans [20] has provided valuable insights into the structure/function relationships within this family of proteins. The third family, currently termed the

Key words: crystal structure; metallo-enzyme; glycerol dehydrogenase; EC 1.1.1.6; glycerol oxidation; Bacillus stearothermophilus

Figure 1. Glycerol Oxidation Scheme

"iron-containing" alcohol dehydrogenases, includes polyol dehydrogenases isolated from bacteria [21] and yeast [22]. This family of enzymes is the least well characterized, and, to date, no structural data have been reported for any enzyme in this group. Analysis of the sequence of B. stearothermophilus glycerol dehydrogenase indicates that it is a member of this iron-containing family. Despite this, the biochemical data clearly point to a dependence on Zn2+ rather Fe2+ for activity. While some members of this iron-containing alcohol dehydrogenase family show a dependence on Fe2+ for activity (e.g., E. coli propanediol oxidoreductase [23]), other members also show Zn2+ dependence (e.g., B. methanolicus methanol dehydrogenase [24]). Thus, it is now clear that this nomenclature is probably inappropriate. Each of the enzymes in this family appears to require a divalent metal ion for catalysis and to distinguish them from the medium-chain polyol dehydrogenase family, which also requires a divalent metal ion; we propose to refer to them under the group heading of the family III metal-dependent polyol dehydrogenases. Further subgroupings under this heading could then be used to differentiate enzymes having more closely related metal binding or biochemical properties.

In this paper, we report the three-dimensional structure of GlyDH to provide structural details of this novel family of polyol dehydrogenases and to provide insights into aspects of the enzyme's catalytic mechanism and substrate and cation specificity.

Results and Discussion

Overall Fold, Secondary Structure, and Location of the \mbox{Zn}^{2+} Ion

The GlyDH subunit has approximate dimensions 60 \times 40 \times 40 Å and consists of a single polypeptide chain of 370 residues. It is composed of 9 β strands (β 1- β 9), 14 α helices (α 1- α 14), 4 3₁₀ helices, and a number of loops, which together fold into 2 domains that are separated by a deep cleft (Figures 2, 3a, and 3b).

The N-terminal α/β domain (residues 1–162) consists of a parallel 6-stranded β sheet, with relative strand order 165423 (absolute strand numbers 296534), flanked by 4 α helices and an additional β strand (β 1). All β strands are connected via α helices, except strands β 6 and β 9, which are separated by a β hairpin (strands β 7, β 8). The fold of the N-terminal domain, while reminiscent of the Rossmann fold commonly found in other dinucleotide binding enzymes [25], is in fact quite distinct in structure due to the radically different connectivity. The C-terminal domain (residues 163-370) comprises two subdomains, each one formed from a bundle of α helices. Helices α 6, α 7, and α 8 form a long antiparallel upand-down helix bundle with a left-handed superhelical twist of approximately 60° around the common axis of the bundle. Helices $\alpha 9-\alpha 14$ form an antiparallel Greek key helix bundle [26] composed of helices α 9, α 10, α 11, α 13, and α 14. Helices α 2 and α 7 are kinked at residues Ala46 and Tyr215, respectively, and can therefore, in principle, be represented as separate shorter α helices.

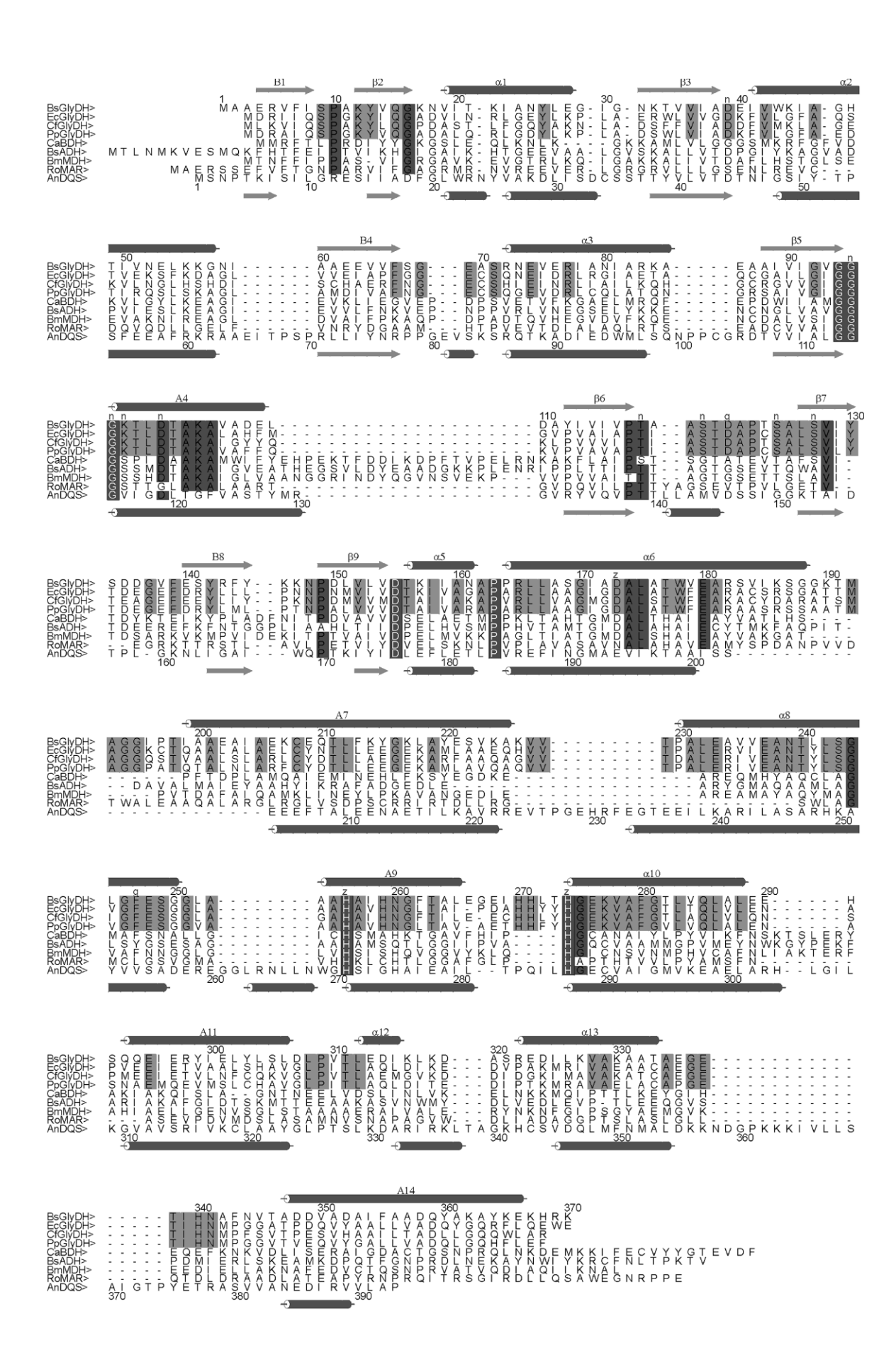
Analysis of the structure shows that a deep cleft is formed between the N- and C-terminal domains, with the Greek key helix bundle and N-terminal domain forming opposing faces of the cleft and the α 6- α 8 bundle forming the floor of the cleft. The Zn²⁺ ion is bound deep in the cleft and is tetrahedrally coordinated through iondipole interaction with amino acid residues Asp173, His256, and His274 and one water molecule (Zn²⁺ Asp173 $O^{\delta 1} = 2.0 \text{ Å, } Zn^{2+} - His256 N^{\epsilon 2} = 2.0 \text{ Å, } Zn^{2+} -$ His274 N^{ϵ 2} = 2.1 Å, and Zn²⁺ – W1 = 1.9 Å) (Figure 3a). The analysis of the pattern of sequence conservation across the family III enzymes shows that the three ligands to the enzyme-bound zinc appear to be conserved in the iron-dependent enzymes of this family, albeit with differences in the flanking sequences (data not shown). At present, therefore, we cannot identify the molecular features that give rise to differences in cation specificity.

Quaternary Structure of Glycerol Dehydrogenase

Previous studies on GlyDH from strain NC1B 11400 have suggested that this enzyme is a tetramer in solution [2]. More recently, gel filtration studies of the GlyDH S305C mutant from *B. stearothermophilus* var. nondiastaticus (strain DSM 2334) have suggested that GlyDH is an octamer in solution [10]. Electron microscopy analysis of both the wild-type and S305C mutant of GlyDH from *B. stearothermophilus* is consistent with a tetrameric structure comprising four subunits related by four-fold symmetry, giving a particle with approximate dimen-

Figure 2. A Multiple, Structure-Based Sequence Alignment of Several Members of the Family III Polyol Dehydrogenases Together with that of Aspergillus nidulans Dehydroquinate Synthase

Amino acid sequences are shown for glycerol dehydrogenases from *B. stearothermophilus* (BsGlyDH, P32816), *Escherichia coli* (EcGlyDH, P32665), *Citrobacter freundii* (CfGlyDH, P45511), *Pseudomonas putida* (PpGlyDH, P50173), for NADPH-dependent butanol dehydrogenase from *Clostridium acetobutylicum* (CaBDH, P13604), for alcohol dehydrogenase from *Bacillus subtitlis* (BsADH, P71017), for NAD+-dependent methanol dehydrogenase from *Bacillus methanolicus* (BmMDH, P31005), for maleylacetate reductase I from *Rhodococcus opacus* (RoMAR, O84992), and for dehydroquinate synthase from *Aspergillus nidulans* (DHQS, PDB1DQS). Amino acid residues that are identical in all sequences are shaded in black and are shown in reversed type. Residues that are conserved in eight of the nine sequences are shaded in dark gray and are shown in normal type. Residues that are identical in all glycerol dehydrogenases are shaded in light gray. The secondary structure of BsGDH and DHQS are shown above and below the sequences, respectively. Amino acid residues that are involved in catalysis by BsGDH are marked by letters above the sequences (n, NAD+ binding; z, Zn²⁺ binding; and g, glycerol binding).



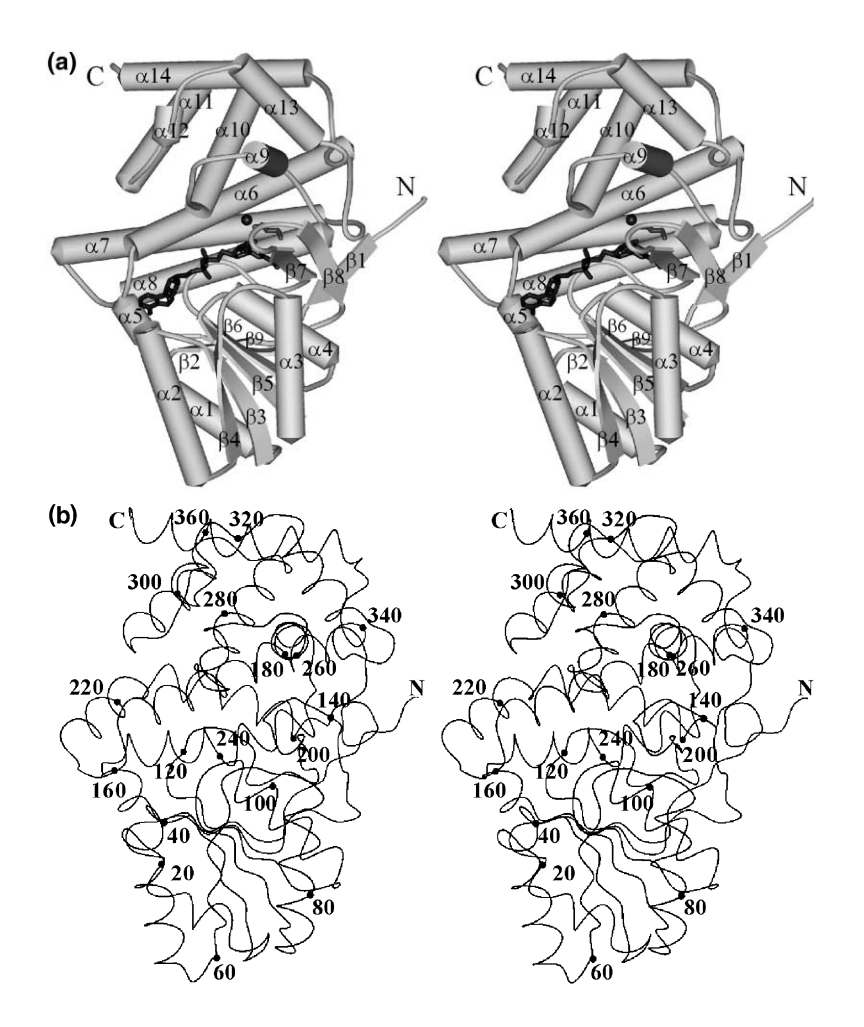


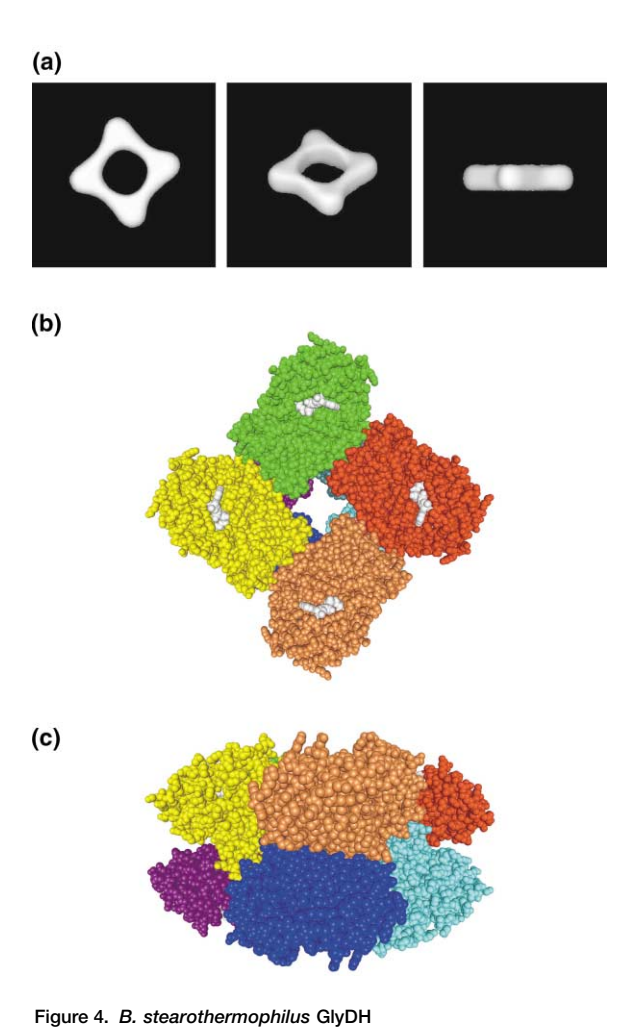
Figure 3. The GlyDH Subunit from *B. stearo-thermophilus*

- (a) A stereo representation of β strands and α helices, which are represented as arrows and rods and are labeled as in the text. The Zn²⁺ ion (gray sphere), NAD⁺, and glycerol are also shown.
- (b) A stereo representation of a C^{α} backbone trace with every 20th residue labeled. The orientation is as in (a).

sions of $105 \times 105 \times 30$ Å and a large hole around the four-fold axis (Figure 4a). A molecular four-fold axis in GlyDH is also supported by the packing in the crystal, with the crystallographic four-fold axis c representing the molecular four-fold axis relating subunits A, B, C, and D in an identical orientation to that observed in the electron microscopy analysis, giving a particle of dimensions 100 imes 100 imes 30 Å. In the crystal, tetramers of GlyDH related by the crystallographic two-fold axes a and b share an extensive buried surface (8.4% of the total solvent accessible area of a subunit), strongly suggesting that this is the surface used in the octamer assembly. Thus, the asymmetric unit of the crystal comprises one subunit of the octamer whose overall dimensions are $100 \times 100 \times 60$ Å (Figure 4). The difference between the quaternary structure observed by electron microscopy on the one hand and X-ray crystallography and gel filtration on the other is not clear. The concentration of the protein solution, when applied to the grids, was \sim 0.1 mg ml $^{-1}$; further dilution occurred upon washing and staining. The concentration of protein used in the gel filtration measurements was \sim 15-20 mg ml⁻¹; this may have been sufficiently high to favor an octameric form over a tetrameric form. Another possibility is that the putative octameric form is unstable at the pH of the negative stain (\sim 5). However, the overall morphology of the electron microscopy-derived tetramer is remarkably similar to that of the subunits related by the crystallographic four-fold axis. Therefore, we believe it is unlikely that the electron microscopy structure represents a collapsed GlyDH octamer.

The GlyDH octamer has 42 symmetry, and analysis of the crystal packing shows extensive interaction between subunits related by the four-fold axis c and the two-fold crystallographic a or b axes. The solventaccessible surface area of an isolated monomer and an octamer have been calculated by using CNS (using the rolling ball method with a probe radius of 1.4 Å [27]) and are 15,200 Å² and 99,600 Å², respectively (figures quoted to the nearest 100 Å2). Thus, upon formation of the octamer, approximately 18% of the solvent-accessible surface is buried per monomer. The interactions around the four-fold axis involve residues from the antiparallel helical bundle (helix α 7 and the turn between helices α 7 and α 8) and the loop between β 2 and α 1 of subunit A and residues from the Greek key helical bundle (helices α 10, α 11, and the loop between them and helix α 14) from subunit B. A total of 4 salt bridges, 3 direct proteinprotein H bonds, and approximately 30 van der Waals contacts form this interface, which buries approximately 700 Å² (4.6%) of solvent-accessible surface per monomer. An equivalent area is buried by the interaction of subunit A with its other four-fold related partner D.

The subunits of GlyDH are related in the crystal by



(a) Views of the electron microscopy structure seen down the fourfold axis, 45° to the four-fold axis, and 90° to the four-fold axis. (b) A space-filling model of the GlyDH octamer with bound cofactor (white) viewed down the four-fold axis.

(c) A space-filling model with the four-fold axis in a vertical orientation.

the crystallographic two-fold axis, which lies at a kink between strands $\beta 1$ and $\beta 2$ of one subunit and results in an antiparallel interaction of these strands with their symmetry-related partners in another subunit. Additional hydrophobic and H bond contacts are present between helices $\alpha 7$ and the loop between $\beta 8$ and $\beta 9$ and their symmetry-related equivalents. A total of 14 direct protein-protein H bonds, 2 salt bridges, and approximately 60 van der Waals interactions form this interface, which buries approximately 1300 Ų (8.6%) of solvent-accessible surface per monomer.

In the crystals of GlyDH, neighboring octamers can be seen to interact via Zn²+-mediated contacts arising from residues in the 3_{10} -helical loop between $\alpha 9$ and $\alpha 10$ in one octamer and the symmetrically equivalent residues in another octamer. The coordination sphere of this Zn²+ ion involves four short and two long interactions (Zn²+ - His271 Ne² = 2.05 Å, Zn²+ - Glu268 Oe² = 2.02 Å, Zn²+ - Glu268 Oe³ = 2.9 Å, and their symmetry equivalents).

Location of the Binding Site for NAD+

The initial crystals of the enzyme were grown in the presence of 10 mM NAD⁺, and analysis of the electron density maps led directly to the identification of a strong electron density feature (Figure 5a) into which an NAD⁺ moiety could be fitted in an unambiguous conformation.

The adenine ring binds in the *anti* conformation with $\chi \approx 117^\circ$ (classification according to [28]) in a pocket on the enzyme surface formed by the residues Ile41, Val42, Ile45, Thr118, Pro163, and Leu166 (Figure 6a). Direct hydrogen bonds are formed between the adenine nitrogen atom at position N6 and the carbonyl oxygen of Thr118 and the side chain of Thr118 at position N7. The adenine ribose appears to be in a C2'-endo conformation, and the ribose O2' hydroxyl group can be seen to be involved in a hydrogen bond with the side chain of Asp39, which lies at the end of strand β 3.

The pyrophosphate moiety of the NAD+ lies close to the loop between $\beta6$ and $\beta7$ (residues 121-122) and interacts with the glycine-rich turn (residues 94-96) that forms the loop between strand β 5 and helix α 4. Hydrogen bonding contacts are made by the pyrophosphate oxygen atoms with the peptide nitrogen atoms of Gly96, Lys97 in this loop, and with the side chain of Ser121 (Figure 6a). The interaction of the pyrophosphate moiety of NAD(P) with a glycine-rich turn and a following α helix is characteristic of the classic recognition of NAD+ by dehydrogenases having a typical Rossmann fold, such as lactate dehydrogenase (LDH) [29]. However, the precise mode of recognition between the nucleotide and LDH and GlyDH is different. While in both GlyDH and lactate dehydrogenase the glycine-rich turn occurs at the C-terminal end of the β strands in the center of the β sheet, the orientation of the nucleotide is quite different. Compared to the nucleotide in lactate dehydrogenase, the nucleotide in GlyDH is rotated by approximately 180° about an axis that lies perpendicular to the β sheet and passes approximately through the pyrophosphate moiety. This results in a modified arrangement in which the edge of the adenine ring and its associated ribose, which are exposed to the solvent in LDH, are buried against the protein surface in the GlyDH, and, furthermore, both groups are displaced to the other side of the glycine-rich turn (Figure 6b). In LDH and GlyDH, an acidic residue at the C-terminal end of a β strand (β 2 and β 3, respectively) adjacent to the strand preceding the glycine-rich turn (β 1 and β 5, respectively) recognizes the adenine ribose hydroxyl groups (Figure 6b). The two β strands that carry the acidic residues (\(\beta 2 \) in LDH and \(\beta 3 \) in GlyDH) are nonequivalent in our superposition, as expected from the difference in the orientation of the NAD+ on the two enzymes. Torsion angle changes in the vicinity of the pyrophosphate moiety result in the same face of the nicotinamide ribose being presented to the enzyme surfaces; but, in both cases, it is clear that the nicotinamide ring lies on the same side of the sheet as the helix that follows the glycine-rich turn (Figure 6b).

The nicotinamide ribose is in a C2′-endo conformation, and hydrogen bonds are formed between the ribose O2′ hydroxyl group and Tyr133 and between the O3′ hydroxyl group and Lys97 and Tyr133 (Figure 6a). The nicotinamide ring is in the anti conformation with $\chi \approx$

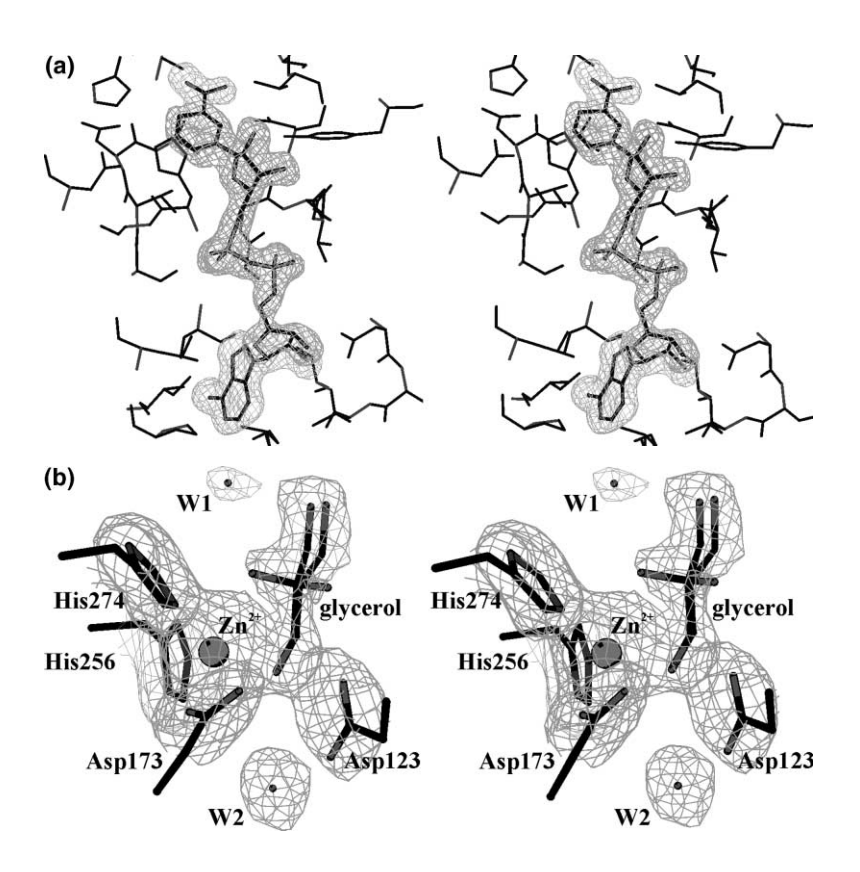


Figure 5. A Stereo Diagram of a Representative Portion of the $|2F_o-F_c|$ Electron Density Map, Contoured at 1.0 σ

- (a) An electron density map for the NAD⁺ bound in the active site of GlyDH, calculated at 1.7 Å resolution.
- (b) An electron density map for the glycerol molecule in the two possible orientations located in the vicinity of the Zn²⁺ ion, calculated at 2.05 Å resolution.

130° and binds in a deep pocket formed by the residues Asp100, Asp123, Ala124, Ser127, Leu129, Val131, Asp173, His174, and Phe247. Direct hydrogen bonds are formed between the carboxyamide nitrogen atom of the nicotinamide ring at position N7 and the side chain atoms of Asp100 and the carbonyl oxygen of Leu129 and between the carboxyamide oxygen atom O7 and the side chain of Ser127. With the nicotinamide ring in this orientation, the B face is packed against the protein surface, with the B hydrogen at position C4 principally shielded by Ala124. In contrast, the A face of the ring from which the proton is abstracted during the enzyme's catalytic cycle is exposed to solvent in the catalytic site. The closest approach of the Zn2+ ion to NAD+ is to the C5 of the nicotinamide ring, which is located \approx 4 Å from the metal ion center.

In order to analyze the nature of any conformational changes associated with NAD+ binding, we have collected data on crystals of free enzyme. Comparison of this structure with that of the GlyDH S305C/NAD+ binary complex revealed that the rmsd between equivalent C^{\alpha} atoms is approximately 0.6 Å. The most obvious consequence of NAD+ binding is a shift of up to 6 Å of the 128-149 loop, part of which (residues 132-138) is partially disordered in the free enzyme. Additionally, residues in the glycine-rich turn (residues 94-103) and the section of polypeptide chain from the end of strand 84 to the end of helix α 3 (residues 66-85) shift by up to 1.4 and 2.3 Å, respectively (Figure 6c). These structural changes serve to optimize the interaction between the enzyme and the NAD+, particularly in the vicinity of the nicotinamide ring.

Glycerol Binding Site

In order to analyze the nature of the binding site for glycerol, we have solved the structure of a binary complex of GlyDH cocrystallized with glycerol. A comparison of this structure with that of the free enzyme revealed that there appears to be no major conformational rearrangements and that the rmsd between equivalent C^{α} atoms is approximately 0.18 Å.

The electron density associated with the glycerol moiety in the structure of GlyDH S305C mutant/glycerol complex is shown in Figure 5b. Inspection of the electron density provides evidence for two possible orientations of glycerol that differ by a rotation of the glycerol around an axis through the molecule, which results in a net displacement of only the O2 oxygen with respect to the protein. The electron density suggests that one of these orientations is preferred (hereafter called the major orientation). The binding of glycerol seems to involve the displacement of three highly ordered water molecules in the binding site, which lie in the vicinity of the Zn2+ ion in the structure of the GlyDH S305C/NAD+ complex. The orientation of the glycerol molecule in the active site is stabilized by van der Waals interaction of the C1 and C3 glycerol carbon atoms with the benzyl ring of Phe247, with additional electrostatic interactions between the negatively charged π -electron cloud of the benzyl ring and the partially positively charged carbon atoms of glycerol.

In this structure, the O1 atom of glycerol forms one ligand to the tetrahedrally coordinated Zn²⁺ ion and is 2.4 Å and 2.9 Å from the Asp123 O^{δ1} and His256 N^{ε2} atoms, respectively, implying a significant interaction. In the major orientation for the glycerol, the O2 atom

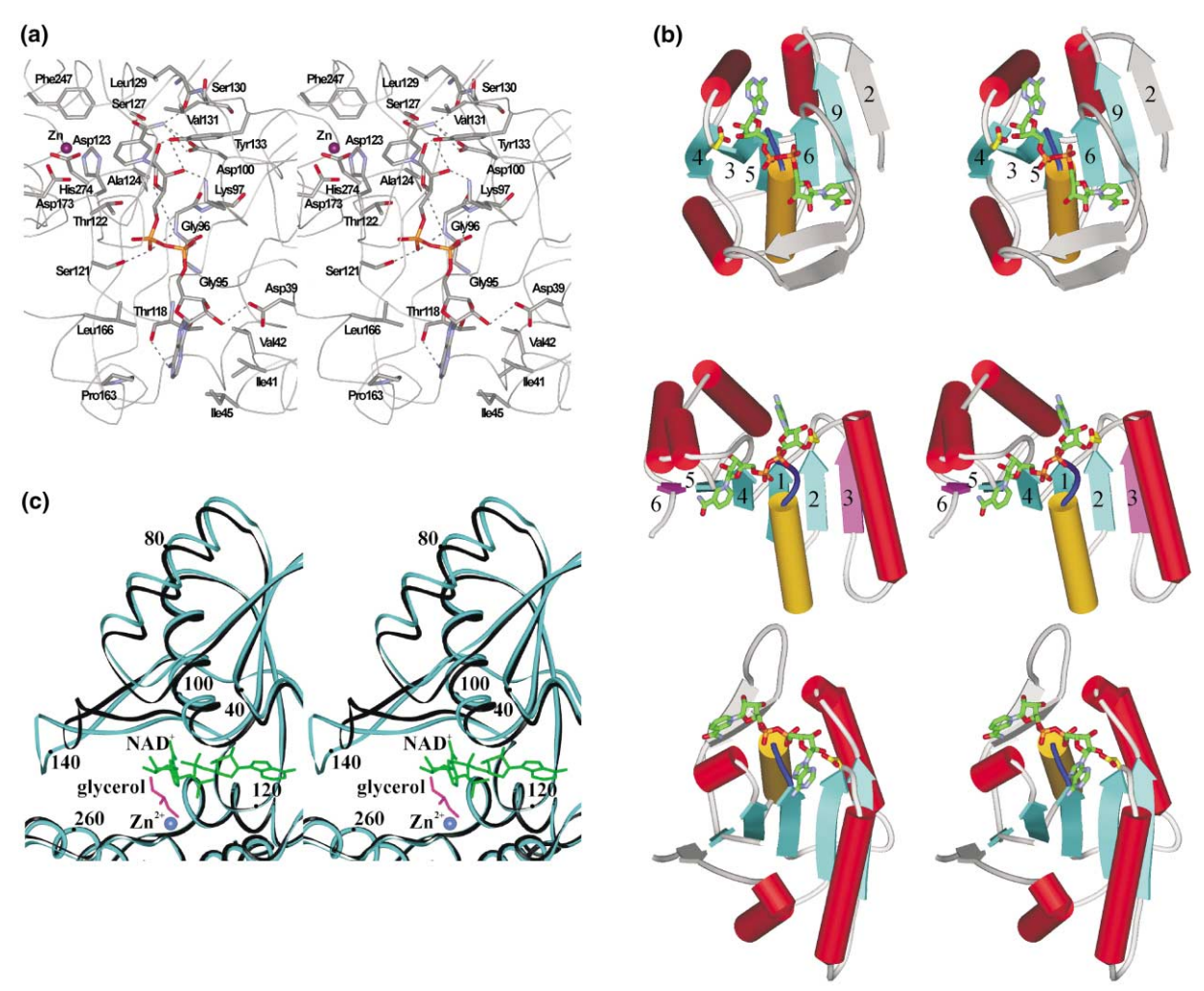


Figure 6. Analysis of the GlyDH/NAD+ Binding Site

(a) A stereo diagram of the NAD⁺ binding site of GlyDH showing the H bond contacts made by the NAD⁺ cofactor with the enzyme surface. All residues involved in an interaction with NAD⁺ are labeled.

(b) A schematic diagram of the NAD⁺ binding domains in GlyDH (top) and lactate dehydrogenase 1LDH (middle) drawn to show the structural equivalence between the two proposed in this paper and oriented such that the glycine-rich turn (dark blue) and the following nucleotide binding helix (yellow) are similarly positioned. The lower figure represents the enzyme DHQS oriented to show the equivalence proposed by Brown and coworkers [33] between this enzyme and LDH. The acidic residues that recognize the adenine ribose hydroxyls in each of the enzymes are shown. β strands in GlyDH and DHQS that have no equivalents in LDH in the respective proposed superpositions are colored gray. Strands 3 and 6 in LDH, which have equivalents in only one or the other of the two possible superpositions alone, are colored pink. (c) Structural changes in the vicinity of the active site of GlyDH caused by NAD⁺ binding. A stereo representation of the superimposed C^{α} trace of the GlyDH S305C mutant (green-blue) and its complex with NAD⁺ (black). The positions of the Zn²⁺ ion (blue), NAD⁺ (green), and glycerol (red) are also shown.

provides a second ligand to the Zn²+ ion and is also involved in three hydrogen bonds with His274 Ne², His256 Ne², and with the water molecule W1. In the minor orientation of glycerol, the O2 atom is involved in a hydrogen bond with Asp123 Oỗ¹ and is adjacent to the plane of the peptide bond Asp123–Ala124. Superposition of the two orientations of glycerol in the enzymecomplex onto the structure of the S305C/NAD+ binary complex would suggest that the minor orientation is not possible in the presence of NAD+ because of steric clashes of the glycerol O2 atom with the nicotinamide ring of NAD+. The O3 glycerol atom is involved in a hydrogen bond with the water molecule W1, which is, in turn, hydrogen bonded to the O2 glycerol oxygen.

The fact that in the major orientation of the glycerol both the O1 and O2 atoms are ligands to the $\rm Zn^{2+}$ ion provides a possible explanation for the substrate specificity of GlyDH that readily utilizes 1,2-diols [2]. This would suggest that the major orientation is the one adopted during catalysis. Further, details of the glycerol binding site are presented in Table 1.

A Possible Mechanism of Glycerol Oxidation

The analysis of the structures of the binary complexes of GlyDH with NAD⁺ and with glycerol has allowed us to produce a model for the productive ternary complex of GlyDH with its substrates (Figure 7a). This model was based on positioning glycerol as observed in the

Table 1. Hydrogen Bond and Electrostatic Interactions, up to 4 Å, of the Bound Glycerol Molecule in the GlyDH S305C/ Glycerol Binary Complex Structure

Glycerol Atom	Protein Atom	Distance (Å)	
01	Zn ²⁺	2.00	
	Asp123 O ^{δ1}	2.41	
	Asp123 O ⁸²	2.98	
	Asp173 O ^{δ1}	3.13	
	Asp173 O ⁸²	3.34	
	His256 N ^{€2}	2.87	
	His274 N ^{€2}	3.87	
	W3 (Thr177 O ^{γ1} , Asp123 O ^{δ2}) ^b	3.77	
O2	Zn ²⁺	2.41	
	His256 N ^{€2}	3.23	
	His274 N ^{€2}	2.75	
	W1 (W2, glycerol O3) ^b	2.78	
O2°	Zn ²⁺	3.74	
	Asp123 O ^{δ1}	2.80	
	Ala124 N	3.66	
O3	W1 (W2, glycerol O2) ^b	2.91	

^a Mean distances are given for the major and minor glycerol orientations and separate values corresponding to the major and minor positions for O2.

structure of its binary complex with GlyDH into an equivalent position in the structure of the binary complex with NAD⁺. The catalytic Zn²⁺ ion is located in the middle of the deep cleft between the enzyme's two domains and becomes totally inaccessible to the solvent as NAD⁺ binds (Figure 7b). This allows the hydride transfer process to take place in an environment that is buried from the solvent.

The pK of the C2 hydroxyl oxygen of glycerol may be lowered considerably by interaction with the enzymebound Zn²⁺ ion. This would allow the hydroxyl proton to be removed possibly via a water molecule-mediated proton shuttle. Subsequent collapse of the resultant alkoxide ion intermediate to the ketone can then proceed with transfer of the hydride from the C2 carbon to the C4 of the nicotinamide ring. To facilitate this, it is clear that the nicotinamide ring is located in a suitable orientation and at a suitable distance (3.2 Å between the glycerol C2 and C4 of the nicotinamide ring of the NAD+) for hydride transfer to occur [30, 31]. Preliminary modeling studies of the binding of dihydroxyacetone to the active site suggest that this substrate can be accommodated in the binding pocket without any major structural changes and with the carbonyl oxygen close to the enzymebound Zn2+ ion.

Structural Similarities with Other Proteins

A structural similarity search, performed with the atomic coordinates of GlyDH using the DALI server [32], indicated that this structure has a close structural similarity to the subunit of Aspergillus nidulans dehydroquinate synthase (DHQS) [33] (PDB accession code 1DQS), with an rmsd of 1.6 Å for the superimposition of 213 C $^{\alpha}$ atoms, which include elements of secondary structures from both domains. Furthermore, the two domains of GlyDH appear to be held in an identical orientation to that seen

in DHQS (Figure 8a). While for the entire sequence a structure-based sequence alignment shows only 14% identity, sequence alignment of the portions of the structures that superimpose well showed 24% identity (over 213 residues). There are no other known structures that have significant structural similarity either to the whole GlyDH subunit or to its separate domains.

DHQS catalyzes the conversion of 3-deoxy-D-arabino-heptulosonate-7-phosphonate (DAHP) to dehydroquinate in a complex multistep mechanism. The first step in this chemistry, the oxidation of a hydroxyl group to a ketone by NAD+ in a Zn2+-dependent process, is similar to that catalyzed by GlyDH. Comparison of the active sites of these enzymes shows them to be closely related with the enzyme-bound Zn2+ of GlyDH occupying an identical position to the catalytic Zn^{2+} in DHQS. Interestingly, the orientation of two hydroxyl groups of a carbaphosphonate inhibitor bound to DHQS is very similar to that seen for the hydroxyl groups of glycerol in the major orientation. Furthermore, two of the three residues in GlyDH that interact with the Zn^{2+} ion (His256 and His274) are conserved in DHQS (His272 and His287, respectively) (Figures 2 and 8b), and the third residue, Asp173, is conservatively substituted by Glu194.

Catalysis by DHQS involves further chemical steps resulting in reoxidation of the enzyme-bound NADH cofactor in a process that involves β-elimination of inorganic phosphate, reduction of the ketone, a ring opening, and an intramolecular aldol condensation. Important residues in this process are thought to be Arg130, Lys152, Asn162, Lys250, Arg264, Asn268, and Lys356. None of these residues are conserved in GlyDH, and, thus, the region of the enzyme responsible for this difference in function is completely altered. Analysis of the active site of DHQS revealed that there were similarities to the arrangements of the residues that mediate alcohol oxidation in the Zn2+-dependent "long-chain" alcohol dehydrogenases. However, the difference in the folding pattern of DHQS and this class of polyol dehydrogenases suggested a convergent evolutionary relationship between them [33]. On the basis of our study, we assume that GlyDH and DHQS are related by divergent evolution from a common ancestor. However, whether the more complex chemistry of DHQS represents that of the ancestor enzyme that was subsequently modified to that of a much simpler polyol dehydrogenase through gene duplication and mutation or vice versa is unclear.

The NAD⁺ binding domain of DHQS [33] is very similar to that seen in GlyDH, with both of them being more similar to each other than they are to the Rossmann fold commonly found in other dinucleotide binding enzymes [25]. Comparison of DHQS with enzymes that have the classical Rossmann fold led Brown and coworkers [33] to suggest that, in DHQS, the nucleotide binds in a different orientation to that in LDH, with the nicotinamide and adenine moieties occupying the opposite faces of the β sheet. The superposition of Brown and coworkers of these two enzymes [33], which led to the above conclusion, followed naturally from the consideration of maximizing the topological equivalence of DHQS and LDH. However, across the family of dehydrogenases that carry the Rossmann fold, only the four central strands of the sheet and a glycine-rich turn that follows the first strand and the following nucleotide binding helix

^bThe table also contains details, as shown in parentheses, of the hydrogen bond partners of the water molecules that interact directly with glycerol.

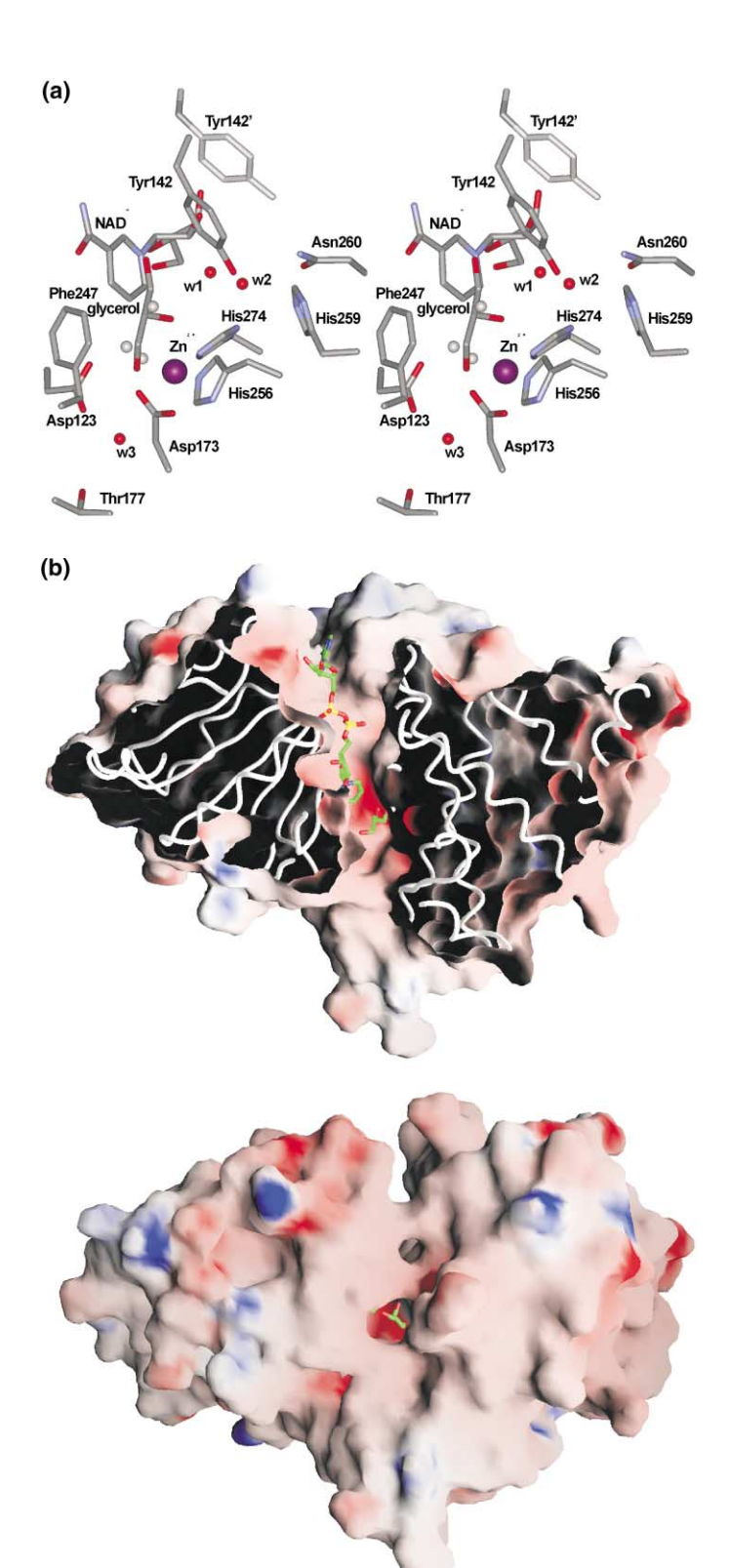


Figure 7. The Active Site of GlyDH

(a) A stereo representation of the model for the ternary complex of B. stearothermophilus GlyDH showing the relative positions of Zn2+ (purple), glycerol, and NAD+. Two positions are shown for Tyr142, corresponding to the movement of this side chain on NAD+ binding. The three water molecules of the free enzyme that are substituted by glycerol in the binary complex are shown as silver spheres. (b) The van der Waals surface of the GlyDH structure as seen in its binary complex with NAD+ shape (GRASP [56] representation) colored according to the electrostatic potential with the NAD+ and glycerol molecules shown in the active site of enzyme. The Zn2+ ion was included in the surface calculation. The two views are approximately at right angles to each other.

are spatially conserved [34]. However, a disadvantage of the structural alignment proposed by Brown and coworkers [33] is that it does not conserve the position of the glycine-rich turn nor of the nucleotide binding helix with respect to their position in LDH.

In the previous discussion of the NAD+ binding site

in GlyDH we have proposed an alternative view of the relationship between this enzyme and the more classical Rossmann fold proteins. Thus, in contrast to the superposition of Brown and coworkers [33], our alternative possible superposition retains the spatial conservation of the glycine-rich turn and the nucleotide binding helix

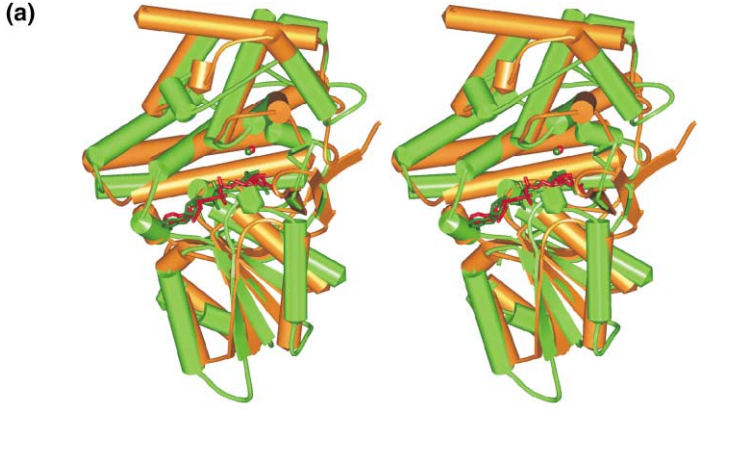
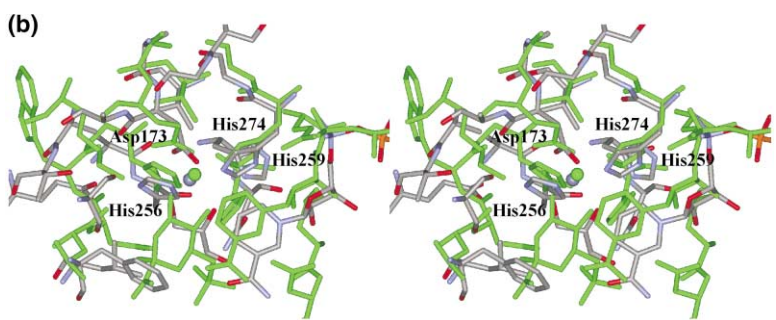


Figure 8. Three-Dimensional Comparison of the GlyDH Structure with *Aspergillus nidulans* DHOS

(a) A stereo representation of the schematic model of a superposition of GlyDH (yellow with NAD $^+$, red with glycerol and Zn $^{2+}$) and DHQS (green with NAD $^+$, dark green with DAHP and Zn $^{2+}$).

(b) A stereo representation of the superposition of the active sites of GlyDH (C, gray; O, red; and N, blue) and DHQS (green). Catalytically important residues of GlyDH are labeled.



but effectively transposes the sequence order of the two mononucleotide binding folds that together comprise the Rossmann fold (Figure 6b) so that it no longer conforms the conventional pattern. Given the absence of sequence similarity between either DHQS and GlyDH on the one hand and LDH on the other, it is not possible to prove which, if either, of the above superpositions represent the evolutionary relationship to LDH. Further, it is not possible to prove with present data if the GlyDH/ DHQS fold is related to the Rossmann fold by divergent or convergent evolution. However, we suggest that our proposed alignment has the advantage of retaining significant functional similarities to the classical Rossmann fold. If this is indeed the case, then the transposition of the two mononucleotide binding folds suggests additional ways in which the domains of NAD+ binding enzymes have evolved. On the other hand, Brown and coworkers' [33] alignment has the advantage of maintaining the overall fold topology.

Therefore, the structure of GlyDH poses two evolu-

tionary conundrums both in terms of the precise origin of the undeniable similarity between GlyDH and DHQS and, more controversially, in terms of the relationship between both enzymes and the wider family of dinucleotide binding enzymes that possess the Rossmann fold. Is it possible that, during evolution, two mononucleotide binding folds assembled in a different sequence order? Does the observation that GlyDH, DHQS, and LDH possess a glycine-rich turn and a nucleotide binding helix provide evidence for aspects of convergent evolution? Alternatively, have GlyDH and DHQS evolved by divergent evolution from an LDH-like fold, with repositioning of the substrate and radical reorganization of the key elements required for substrate binding? Currently, we cannot answer these intriguing questions. However, it is possible that, in the future, as part of the global survey of protein folds that will result from initiatives in structural genomics, other variants of this fold will be observed and will help resolve the question of the origin of these proteins one way or another.

Table 2. Heavy Atom Derivatives, X-Ray Data Collection, and Phasing Statistics

	-					
Data Set	Pt ^I	Pt ^{II}	Pt ^{III}	Pt ^{IVa}	Au	U
Heavy atom reagent	K ₂ PtCl ₄	K ₂ Pt(NO ₃) ₄	K ₂ PtCl ₄ /K ₂ Pt(NO ₃) ₄	K ₂ PtCl ₄ /K ₂ Pt(NO ₃) ₄	KAu(CN) ₂	UAc
Resolution (Å)/R _{merge} ^b (%)	3.5/6.2	4.5/4.3	2.8/9.0	2.5/6.6	2.7/5.3	4.5/5.8
Completeness (%)	99.6	99.7	62.4	70.3	99.3	98.9
MFID° (%)	6.1	9.8	17.4	15.8	8.6	13.5
Phasing powerd (acentric/centric)	0.88/0.67	1.31/0.91	1.93/1.39	1.40/0.96	0.62/0.40	0.73/0.51

^aThe data set was collected from two crystals.

 $^{{}^{}b}R_{meroe} = \sum_{hkl} |I_i - I_m| / \sum_{hkl} I_m$, where I_m is the mean intensity of the reflection.

[°]Mean fractional isomorphous difference = $\Sigma ||F_{PH}| - |F_P||/\Sigma |F_P|$, where F_{PH} and F_P are the structure factor amplitudes for derivative and native crystals, respectively.

^d Phasing power is defined as the rms value of heavy atom structure factor amplitude divided by the rms value of lack-of-closure error.

Table 3. Refinement Statistics			
Data set	Native	NAD ⁺	glycerol
Resolution (Å)	10.0-1.8	10.0–1.7	10.0-2.05
Observed reflections	194,595	196,167	104,049
Number of reflections used ^a	34,153	41,600	24,761
Completeness ^b (%)	89.6 (83.4)	92.1 (78.6)	92.9 (72.0)
R _{merge} ^{b,c} (%)	6.4 (41.5)	4.7 (37.6)	8.1 (28.8)
I/sigI ^b	13.6 (2.7)	19.9 (2.7)	13.2 (2.9)
R _{cryst} (%) ^d /R _{free} (%) ^e	16.3/20.8	15.1/19.0	15.8/20.2
Refinement model number of atoms			
Protein atoms	2713	2749	2719
Ions	2	2	2
Substrate	_	44	6
Water molecules	239	271	174
Mean B values (Ų)			
Protein atoms ^f	33.5 (30.4)	29.0 (25.7)	35.5 (32.3)
Water	50.6	46.5	46.4
Catalytic Zn ²⁺	23.0	17.9	22.9
Crystal contact Zn2+	33.7	28.9	42.5
NAD(H)	-	34.0	_
Glycerol	_	_	44.5

^a Data with F_0 /sigma(F_0) less than 1σ are omitted.

Biological Implications

Under anaerobic conditions, many microorganisms utilize glycerol as a source of carbon through coupled oxidative and reductive pathways. This is done through oxidation of glycerol and is catalyzed by glycerol dehydrogenase, leading to the formation of dihydroxyacetone (1,3-dihydroxypropanone) with concomitant reduction of NAD⁺ to NADH. The dihydroxyacetone is then phosphorylated by dihxydroxyacetone kinase to enter the glycolytic pathway for further degradation.

We describe here the structure of glycerol dehydrogenase from *B. stearothermophilus*, the first for any member of the so-called "iron-containing" polyol dehydrogenase family. Analysis of the mode of NAD⁺ binding has allowed us to propose a possible mechanism of glycerol oxidation and provides an explanation for the substrate specificity of GlyDH that readily utilizes a wide range of 1,2-diols.

Structure comparisons reveal that the fold of GlyDH is remarkably similar to that of Aspergillus nidulans dehydroquinate synthase, despite the fact that these enzymes share only 14% sequence identity. While DHQS carries a more complex chemistry than GlyDH, they share a common chemical step, thereby providing a striking example of divergent evolution. The fold of the N-terminal NAD+ binding domain of GlyDH is reminiscent of the Rossmann fold commonly found in other dinucleotide binding enzymes. However, one of two ways of superimposing the GlyDH structure on LDH retains the spatial equivalence of key elements involved in NAD+ recognition but alters the relative sequence order of the two mononucleotide binding folds. This has potential implications for understanding the evolutionary origins of this type of domain.

Experimental Procedures

Site-Directed Mutagenesis

The S305C mutation was achieved by the methods of Kunkel [35], using wild-type GlyDH DNA [12] cloned into M13mp18 as the template. The antisense primer used was 5'-TGGCAAATCAAGGCACAA ATAAAGCTC-3', with the mismatched codon highlighted in bold. The mutation was confirmed by DNA sequencing using the Sequenase 2.2 DNA sequencing kit (United States Biochemical Corporation), and the mutated gene was subcloned into pKK233-2 for expression in *E. coli* JM103.

Studies on the S305C mutant enzyme used in these studies showed that its Km values for glycerol and NAD $^+$ are 4.1 \pm 0.45 mM and 99.8 \pm 3.1 μ M, respectively, very close to those of the wild-type enzyme (3.8 \pm 0.37 mM and 121 \pm 3.1 μ M, respectively) under the same conditions. Its specific activity was found to be 22.5 IU, close to that determined previously for the wild-type enzyme [2].

Electron Microscopic Studies

A sample solution of the GlyDH S305C mutant (0.15 mg ml $^{-1}$) was adsorbed on a thin carbon film supported on a 400-mesh copper/palladium grid for 1 min, washed twice, negatively stained with 1% uranyl formate (pH \sim 5), blotted, and air dried. Electron micrographs were recorded on a Philips CM 100 microscope operating at 100 kV at a magnification of 50,000 \times in bright-field mode. Two exposures of the same field of view were recorded: the first one was taken at a nominal 45° tilt angle, followed by a second one at 0°. Images were recorded at an underfocus of \sim 5000 Å.

All particle images were selected from three pairs of tilted and untilted micrographs. The micrographs were digitized with a Zeiss SCAI scanner with a step size of 28 μm , corresponding to 5.6 Å on the specimen scale. The optical transmission measured with this instrument was converted into optical density values. Particles were windowed in 64 \times 64-pixel boxes. Image processing was performed with the SPIDER software system [36]. A bandpass filter with Gaussian smoothed edges was applied to a total of 2200 image pairs in order to suppress both high frequencies beyond 1/15 Å and low frequencies below 1/200 Å. All particle images were normalized to zero mean and masked with a smooth-edged circular mask and a diameter of 40 pixels.

In the untilted images, the particles were found in predominantly

^b Numbers in parentheses indicate values for the highest resolution shell.

 $^{{}^{\}rm c}{\rm R}_{\rm merge}=\Sigma_{\rm hkl}{\it I}_{\it i}-{\it I}_{\it m}{\it I}/\Sigma_{\rm hkl}{\it I}_{\it m}$, where ${\it I}_{\it m}$ is the mean intensity of the reflection.

 $^{{}^{}d}\mathbf{R}_{cryst} = \Sigma_{hkl}(|\mathbf{F}_{o}| - |\mathbf{F}_{c}|)/\Sigma_{hkl}|\mathbf{F}_{o}|.$

^e R_{free} was calculated on 5% of the data omitted by random.

¹The B values for the main chain protein atoms alone are given in parentheses.

one orientation. Alignment and classification was performed on all the particles as one group. For the first alignment run, a well-preserved particle with clear four-fold symmetry was used as a reference for alignment of the untilted particles. Using correlation techniques, translational and rotational differences of all images with respect to the reference were corrected. The structural resolution common to all particles was estimated by the use of Fourier Ring correlation and phase residual measurements [38]. The average image of the aligned particles served as the reference for a second alignment step, and the resolution limit was calculated to be 22 Å for the averaged projection image of the protein.

The image set was subjected to correspondence analysis [37, 38]. The first six factors determined from the correspondence analysis were used in the classification step. Four classes were generated, the most populated class of 886 particles displaying an unambiguous four-fold symmetry. Particles belonging to this class were selected for the three-dimensional reconstruction.

The random conical tilt method [39] was applied to reconstruct the three-dimensional structure from the centered tilted particles. The parameters of the alignment procedure on the untilted particles, i.e., the rotation angle of each particle with respect to the reference, combined with the known tilt angle of the tilted micrographs were used to calculate the projection direction of the corresponding view in the tilted exposure. Reconstruction was performed using a weighted back-projection algorithm [40, 41]. The final resolution of the three-dimensional structure was \sim 37 Å. At this resolution, the handedness of the structure cannot be distinguished.

Crystallization and X-Ray Structure Solution

Crystals of the GlyDH S305C mutant were grown by the hanging-drop vapor-diffusion method, using ammonium sulphate and PEG 400 as a precipitating agent with the addition of ZnCl₂ and in the presence and absence of NAD $^+$, as previously described [10]. Crystals of the GlyDH S305C complex with glycerol were obtained by cocrystallization of the enzyme under identical conditions to those described for the free enzyme, but with the addition of 0.3% w/v glycerol. All crystals belong to space group I422, with closely related cell dimensions (a = b = ≈105 Å, c = ≈149 Å). The superior diffraction of these crystals [10], compared to that of the wild-type enzyme [42], combined with the fact that the catalytic properties of the mutant and wild-type enzymes are essentially identical led us to preferentially investigate the structure of the mutant.

The structure of the GlyDH S305C/NAD+ complex was solved using the method of multiple isomorphous replacement with six heavy atom derivatives, prepared by soaking crystals in mother liquor containing the heavy atom reagents in addition to 10 mM NAD+ (Table 2). Diffraction data for derivatives Pt¹, Ptⁿ, Au, and U were collected from a single crystal using a MAR345 image plate detector and platinum/nickel mirror-focused Culα X-rays produced with a Rigaku Ru2000 rotating-anode generator. Data sets for the free enzyme, the Pt¹ derivative, and the binary complexes with NAD+ or glycerol were collected on a Quantum4 CCD detector at the SRS Daresbury laboratory on station 14.2, 9.2, 14.2, and 9.6, respectively. All the data were processed and scaled using DENZO/SCALEPACK [43] and were subsequently handled using CCP4 software [44]. Data collection statistics are summarized in Tables 2 and 3.

The major platinum site was determined from the isomorphous difference Patterson synthesis for the Pt¹ derivative, and an initial phase set was calculated. The locations of the heavy atom sites for all other derivatives were determined by difference Fourier methods. Refinement of heavy atom parameters and phase calculations was carried out with MLPHARE [44, 45]. The combination of derivatives gave an overall figure of merit of 0.46 (acentric 0.44, centric 0.61) for 13,826 reflections between 15.0 and 2.5 Å. An improved map was obtained by combined solvent flattening and histogram matching using the program DM [44], with a solvent content of 43.5%. The overall figure of merit of the resulting phase set after phase improvement procedure was 0.85.

A partial (95%) model of GlyDH was built from this map using TURBO-FRODO [46] and O [47]. After refinement with CNS [48] (R factor = 0.30, $R_{free} = 0.35$), phases from this partial model and the isomorphous replacement phases were combined and extended up to 2.2 Å in SIGMAA [49] to generate an improved map. The model

was then submitted to maximum likelihood and residual refinement using CNS [48]. Only data with cutoff $F_0/sigma(F_0) > 1$ were used in refinement, and a low-resolution cutoff was applied at 10.0 Å. A correction for the disordered solvent continuum was also applied [50]. Geometric data for NAD $^+$ and glycerol were obtained from [51] force constants, and charge distributions were derived from those available within CNS [52].

Refinement of the binary complex with glycerol and the free S305C enzyme was carried out using the structure of the GlyDH S305C/NAD⁺ complex as a starting model. The refinement procedures for all structures were similar to those described above.

In the final model of the binary complex with NAD $^+$, all residues are present, except two residues at the N terminus and three residues at the C terminus. In the refined structure of the free enzyme and complex with glycerol, the equivalent residues are also disordered. However, in addition, the loop between $\beta 7$ and $\beta 8$ (residues 132–140) is also partially disordered, and some of these residues have also been omitted. Typical rmsd on bond length and bond angles for the refinement structures are 0.01 Å and 1.5 $^\circ$, respectively. No residues lie in disallowed regions on the Ramachandran plot.

The calculation of rmsd of bond length and bond angles was carried out by CNS [48]. Analysis of the stereochemical quality of the models was accomplished using PROCHECK [53]. The refinement statistics are summarized in Table 3, and a representative part of the electron density map is shown in Figure 5. Superposition of different structures was carried out by Swiss-PdbViewer [54]. The sequence alignment was carried out with the help of ALSCRIPT [55].

Acknowledgments

We thank the support staff at the Synchrotron Radiation Source at the CCLRC Daresbury Laboratory for assistance with station alignment. This work was supported by the New Energy and Industrial Development Organization, the Wellcome Trust, and Biotechnology and Biological Sciences Research Council (BBSRC). Electron microscopy received generous financial support from the Wolfson Foundation, the Royal Society, FEI UK (formerly Philips Electron Optics), AstraZeneca, Procter and Gamble Pharmaceuticals, and Merck Sharpe and Dohme. The Krebs Institute is a designated BBSRC Biomolecular Science Centre and a member of the North of England Structural Biology Centre.

Received: January 29, 2001 Revised: July 11, 2001 Accepted: July 30, 2001

References

- Scharschmidt, M., Pfleiderer, G., Metz, H., and Brummer, W. (1983). Isolation and characterization of glycerol dehydrogenase from *Bacillus megaterium*. Hoppe-Seyler's Z. Physiol. Chem. 364, 911–921.
- Spencer, P., Bown, K.J., Scawen, M.D., Atkinson, T., and Gore, M.G. (1989). Isolation and characterisation of the glycerol dehydrogenase from *Bacillus stearothermophilus*. Biochim. Biophys. Acta 994, 270–279.
- Viswanath-Reddy, M., Pyle, J.E., and Branch-Howe, H. (1978). Purification and properties of NAD⁺-linked glycerol dehydrogenase from *Neurospora crassa*. J. Gen. Microbiol. 107, 289–296.
- May, J.W., and Sloan, J. (1981). Glycerol utilization by Schizosaccharomyces pombe: dehydration as the initial step. J. Gen. Microbiol. 123, 183–185.
- Morgunov, I.G., and Ilchenko, A.P. (1995). Isolation, purification, and some properties of glycerol dehydrogenase from the yeast Candida valida. Biochem-Moscow 60, 659–664.
- Kormann, A.W., Hurst, R.O., and Flynn, T.G. (1972). Purification and properties of an NADP⁺ dependent glycerol dehydrogenase from rabbit skeletal muscle. Biochim. Biophys. Acta 258, 40–55.
- Lin, E.C.C. (1976). Glycerol dissimilation and its regulation in bacteria. Annu. Rev. Microbiol. 30, 535–578.
- Forage, R.G., and Lin, E.C.C. (1982). Dha system, mediating aerobic and anaerobic dissimilation of glycerol in Klebsiella pneumoniae NCIB 418. J. Bacteriol. 151, 591–599.

- Mallinder, P.R., Pritchard, A., and Moir, A. (1992). Cloning and characterization of a gene from *Bacillus stearothermophilus* var. non-diastaticus encoding a glycerol dehydrogenase. Gene 110, 9–16.
- Burke, J., et al., and Rice, D.W. (2001). Purification, crystallization and quaternary structure analysis of a glycerol dehydrogenase S305C mutant from *Bacillus stearothemophilus*. Acta Crystallogr. D 57, 165–167.
- Blattner, F.R., Burland, V., Plunkett, G., Sofia, H.J., and Daniels, D.L. (1993). Analysis of the *Esherichia coli* genome. 4. DNAsequence of the region from 89.2 to 92.8 minutes. Nucleic Acid Res. 21, 5408–5417.
- Eklund, H., et al., and Akeson, A. (1976). Three-dimensional structure of horse liver alcohol dehydrogenase at 2.4 Å resolution. J. Mol. Biol. 102, 27–59.
- Hurley, T.D., Bosron, W.F., Hamilton, J.A., and Amzel, L.M. (1991). Structure of human β-1,β-1-alcohol dehydrogenase: catalytic effects of non-active-site substitutions. Proc. Natl. Acad. Sci. USA 88, 8149–8153.
- Persson, B., Krook, M., and Jornvall, H. (1991). Characteristics of short-chain alcohol dehydrogenases and related enzymes. Eur. J. Biochem. 200. 537–543.
- Schwartz, M., and Jornvall, H. (1976). Structural analyses of mutant and wild-type alcohol dehydrogenases from *Drosophila* melanogaster. Eur. J. Biochem. 68, 159–168.
- Morris, H.R., Williams, D.H., Midwinter, G.G., and Hartley, B.S. (1974). A mass spectrometry sequence study of the enzyme ribitol dehydrogenase from *Klebsiella aerogenes*. Biochem. J. 141, 701–713.
- Agarwal, A.K., Monder, C., Eckstein, B., and White, P.C. (1989).
 Cloning and expression of rat cDNA-encoding corticosteroid
 11-β-dehydrogenase. J. Biol. Chem. 264, 18939–18943.
- Peltoketo, H., Isomaa, V., Maentausta, O., and Vihko, R. (1988).
 Complete amino acid sequence of human placental 17β-hydroxysteroid dehydrogenase deduced from cDNA. FEBS Lett. 239, 73–77.
- Fisher, M., Kroon, J.T.M., Martindale, W., Stuitje, A.R., Slabas, A.R., and Rafferty, J.B. (2000). The X-ray structure of *Brassica* napus β-keto acyl carrier protein reductase and its implications for substrate binding and catalysis. Structure 8, 339–347.
- Ghosh, D., et al., and Orr, J.C. (1991). The 3-dimensional structure of holo 3-alpha,20-β-hydroxysteroid dehydrogenase: a member of a short chain dehydrogenase family. Proc. Natl. Acad. Sci. USA 88. 10064–10068.
- Scopes, R.K. (1983). An iron-activated alcohol dehydrogenase. FEBS Lett. 156, 303–306.
- Williamson, V.M., and Paquin, C.E. (1987). Homology of Saccharomyces cerevisiae ADH4 to an iron-activated alcohol dehydrogenase from Zymomonas mobilis. Mol. Gen. Genet. 209, 374–381.
- Chen, Y.M., Lu, Z., and Lin, E.C. (1989). Constitutive activation
 of the fucAO operon and silencing of the divergently transcribed
 fucPIK operon by an IS5 element in *Escherichia coli* mutants
 selected for growth on L-1,2-propanediol. J. Bacteriol. 171,
 6097–6105.
- de Vries, G.E., Arfman, N., Terpstra, P., and Dijkhuizen, L. (1992).Cloning, expression, and sequence analysis of the *Bacillus methanolicus* C1 methanol dehydrogenase gene. J. Bacteriol. 174, 5346–5353.
- Birktoft, J.J., and Banaszak, L.J. (1984). Structure-function relationships among nicotinamide-adenine dinucleotide dependent oxidoreductases. In Peptide and Protein Reviews, M.T.W. Hearn, ed. (New York: Dekker), pp. 1–46.
- Richardson, J.S. (1981). The anatomy and taxonomy of protein structure. Adv. Protein Chem. 34, 167–339.
- Lee, B., and Richards, F.M. (1971). The interpretation of protein structures: estimation of static accessibility. J. Mol. Biol. 55, 379–400.
- IUPAC-IUB Joint Commission on Biochemical Nomenclature (JCBN) (1983). Abbreviations and symbols for the description of conformations of polynucleotide chains. Eur. J. Biochem. 131, 9–15.
- 29. Grau, U.M., Trommer, W.E., and Rossmann, M.G. (1981). Structure of the active ternary complex of pig heart lactate dehydro-

- genase with S-lac-NAD at 2.7 Å resolution. J. Mol. Biol. 151, 289-307.
- Bürgi, H.B., and Dunitz, J.D. (1983). From crystal statics to chemical dynamics. Acc. Chem. Res. 16, 153–161.
- Wilkie, J., and Williams, I.H. (1995). Geometrical preferences for general acid-catalysed hydride transfer: comparative theoretical study of transition structures for reduction of formaldehyde.
 J. Chem. Soc. Perkin Trans. 2, 1559–1567.
- Holm, L., and Sander, C. (1995). Dali: a network tool for protein structure comparison. Trends Biochem. Sci. 20, 478–480.
- Carpenter, E.P., Hawkins, A.R., Frost, J.W., and Brown, K.A. (1998). Structure of dehydroquinate synthase reveals an active site capable of multistep catalysis. Nature 394, 299–302.
- Baker, P.J., Britton, K.L., Rice, D.W., Rob, A., and Stillman, T.J. (1992). Structural consequences of sequence pattern in the fingerprint region of the nucleotide binding fold. J. Mol. Biol. 228, 662–671.
- Kunkel, T.A. (1985). Rapid and efficient site-specific mutagenesis without phenotypic selection. Proc. Natl. Acad. Sci. USA 82, 488–492.
- Frank, J., Shimkin, B., and Dowse, H. (1981). SPIDER a modular software system for image processing. Ultramicroscopy 6, 343–358.
- Van Heel, M., and Frank, J. (1981). Use of multivariate statistics in analyzing the images of biological macromolecules. Ultramicroscopy 6, 187–194.
- Frank, J., and Van Heel, M. (1982). Correspondence analysis of aligned images of biological particles. J. Mol. Biol. 161, 134–137.
- Radermacher, M., Wagenknecht, T., Vershoor, A., and Frank, F. (1987). Three-dimensional reconstruction from a single-exposure, random conical tilt series applied to the 50S ribosomal subunit of *Escherichia coli*. J. Microsc. 146, 113–136.
- Vainshtein, B.K. (1971). Finding the structure of objects from projections. Sov. Phys. Crystallogr. 15, 781–787.
- Gilbert, P. (1972). Iterative methods for the three-dimensional reconstruction of an object from projections. J. Theor. Biol. 36, 105, 117.
- Wilkinson, K.W., Baker, P.J., Rice, D.W., and Stillman, T.J. (1995). Crystallization of glycerol dehydrogenase from *Bacillus stearothermophilus*. Acta Crystallogr. D 15, 830–832.
- Otwinowski, Z., and Minor, W. (1997). Processing of X-ray diffraction data collected in oscillation mode. Methods Enzymol. 276, 307–326.
- Collaborative Computational Project No. 4 (1994). The CCP4 suite: programs for protein crystallography. Acta Crystallogr. D 50, 760–763.
- Otwinowski, Z. (1991). Maximum likelihood refinement of heavy atom parameters in isomorphous replacement and anomalous scattering. In Proceeding of the CCP4 Study Weekend, W. Wolf, P.R. Evans, and A.G.W. Leslie, eds. (Warrington, UK: Daresbury Laboratory), pp 80–86.
- Roussel, A., and Cambillav, C. (1991). Silicon Graphics Geometry Partners Directory 86. (Mountain View, CA: Silicon Graphics).
- Jones, T.A., Zou, J.Y., Cowan, S.W., and Kjeldgaarsd, M. (1991). Improved method for building protein models in electron density maps and the location of error in these models. Acta Crystallogr. A 47, 110–119.
- Brünger, A.T., et al., and Warren, G.L. (1998). Crystallography & NMR system: a new software suite for macromolecular structure determination. Acta Crystallogr. D 54, 905–921.
- Read, R.J. (1986). Improved Fourier coefficients for maps using phases from partial structures with errors. Acta Crystallogr. A 42, 140–149.
- Jiang, J.S., and Brünger, A.T. (1994). Protein hydration observed by X-ray diffraction. Solvation properties of penicillopepsin and neuraminidase crystal structures. J. Mol. Biol. 243, 100–115.
- Kleywegt, G.J., and Jones, T.A. (1998). Databases in protein crystallography. Acta Crystallogr. D 54, 1119–1131.
- Parkinson, G., Vojtechovsky, J., Clowney, L., Brünger, A.T., and Berman, H.M. (1996). New parameters for the refinement of nucleic acid containing structures. Acta Crystallogr. D 52, 57–64.
- Laskowski, R.A., MacArthur, M.W., Moss, D.S., and Thornton, J.M. (1993). PROCHECK: a program to check the stereochemi-

- cal quality of protein structures. J. Appl. Crystallogr. 26, 283-291.
- Guex, N., and Peitsch, M.C. (1997). SWISS-MODEL and Swiss-PdbViewer: an environment for comparative protein modelling. Electrophoresis 18, 2714–2723.
- 55. Barton, G. (1993). ALSCRIPT: a tool to format multiple sequence alignments. Protein Eng. 6, 37–40.
- Nicholls, A., Sharp, K., and Hong, B. (1991). Protein folding and association: insights from the interfacial and thermodynamic properties of hydrocarbons. Proteins Struct. Funct. Genet. 11, 281–296.

Accession Numbers

The coordinates of GlyDH S305C and its complexes with NAD^+ and glycerol have been deposited in the Protein Data Bank with accession codes 1JPU, 1JQ5, and 1JQA, respectively.